Mapping Water Bodies from RADARSAT Imagery

Jonathan Li[1]*, Gangyao Kuang[2], Zhiguo He[2]

[1]Department of Geography and Environmental Management

University of Waterloo, Waterloo, Ontario, Canada N2L 3G1

[2]School of Electronic Science and Engineering

National University of Defense Technology, Changsha, Hunan, China

*Corresponding author: junli@uwaterloo.ca

Abstract. *This paper presents a novel geodesic active contour (GAC) model based on an edge detector for rapid detecting of water bodies from spaceborne synthetic aperture radar (SAR) imagery with high speckle noise. The original edge indicator function based on gradients is replaced by an edge indicator function based on the ratio of exponentially weighted averages (ROEWA) operator. Thus, the capability of edge detection and the accuracy of locating edges are greatly improved, which makes the model more appropriate for SAR images. In addition, an enhancing term is added to the original model's energy function in order to boost the strength for the contour's evolution. An unconditionally stable additive operator splitting (AOS) scheme and a fast algorithm for re-initialization of the level set function are adopted, which not only enhances the model's stability, but also speeds up the model's convergence remarkably. The experimental results on RADARSAT-2 images show its efficiency and accuracy.*

1. Introduction

Water resources play an important role in environmental, transportation and regional planning, disaster management, industrial and agricultural production. Detecting water bodies is the first step for any planning, especially for Ontario, Canada, where the land-cover is dominated by water bodies. Spaceborne synthetic aperture radar (SAR) images, when used jointly with in situ data, can provide an essential contribution for the creation of inventories of surface water resources, the extraction of thematic maps relevant for hydrogeographical studies and models [*Shultz and Engman*, 2000]. SAR data are suitable for mapping water bodies, as the signal is principally sensitive to moisture and to surface roughness. These data can be preferred to optical imagery taking into consideration the cloud

penetration capabilities that are fundamental when mapping transient waters typically associated to rainy periods. However, speckle noise usually occurs in SAR images due to the nature of coherent imaging. It makes feature extraction from SAR image much more difficult than that from optical imagery. In order to eliminate the speckle effects, a significant research effort has been devoted to the design of effective segmentation methods over last few decades. Among them, four types of the segmentation methods have been commonly used, namely, the edge-based scheme[*Oliver et al.* 1996; *Collins and Kopp* 2008], the Markov random field (MRF) model [*Fjortoft et al*. 2003], level set theory [*Shu et al.* 2010], and the region merging / region growing family of methods [*Cook et al.* 1994]. The edge-based scheme aims to find transitions between *uniform* areas, rather than directly identifying them. The algorithms based on this technique generally use an edge detection operator. However, it has been shown that these edge-based detectors introduce a bias and increase the variance in the estimation of the edge position when the window does not have the same orientation as the edge [*He* 2008]. The MRF model presents many interesting properties since it allows designing segmentation techniques by taking into account the nature of the fluctuations in a statically optimal way. However, the MRF model introduces several parameters which cannot be easily determined automatically, and may lead to a difficult optimization problem. The narrow band level set segmentation method presented by *Shu et al.* (2010) uses thresholding combined with morphological filtering to segment SAR imagery into land and water followed by refining the segmentation results using level set theory. The region merging methods, such as the merge using moments (MUM) method [*Cook et al.* 1994], use the statistical properties of adjoining regions to merge similar regions. Although these methods usually produce acceptable segmentation results for large textured areas they do not perform well for small targets. Besides, the choice of the parameters can affect the final segmentation.

In recent years, segmentation methods based on active contours have gained tremendous popularity [*Kass et al.* 1988; *Cohen* 1991; *Sethian* 1996; *Zhu and Yuille* 1996; *Caselles et al*. 1997; *Osher and Sethian* 1998]. Active contours were initially introduced in the form of *snakes* by *Kass et al*. [1998]. The method aims at segmenting an image by deforming an initial contour towards the edge of the object of interest. This is done by deforming an initial contour in such a way that it minimizes an energy functional defined on contours. Despite its success, the original parametric active contour model has two noticeable drawbacks. First, it depends on the parameterization of the evolving contour and thus is not geometrically intrinsic. Second, it cannot naturally handle changes in the topology of

the evolving contour. These drawbacks were addressed by the geodesic active contour (GAC) model [*Caselles et al*. 1997]. In this model, the energy functional is minimized as a geodesic computation in a Riemann space. Also, the evolving contours are embedded in a higher-dimensional level set function [*Osher and Sethian* 1998]. This model can easily handle segmentation of several objects, since its level set implicit surface representation remains continuous even if the contours split. However, wrong segmentation results may be produced when the model is applied to SAR imagery. The reason may be that the GAC model exploits a gradient operator to detect edges and the edge map based on gradients is disordered in SAR imagery. Classical differential edge detectors are not well adapted to SAR imagery since their false alarm rate depends on the mean reflectivity: they usually detect more false edges in the areas of high reflectivity than that of low reflectivity [*Touzi el al*. 1988; *Germmain and Refregier* 2001]. Hence, edge detectors specific for SAR images have been developed. The common property of these detectors is that they compute the ratio of averages instead of the difference. *Bovik* [1988] and *Touzi* [1988] defined filters which compute the normalized ratio of averages (ROA). *Fjortoft* et al. [1998] derived a filter from a stochastic image model, whose expression is a modified version of *Shen and Castan* [1992] - the ratio of exponentially weighted averages is considered. In the framework of statistical decision theory, *Oliver et al.* [1996] determined an optimal filter, based on the likelihood ratio (LR) principle. The ROA and LR operators use the arithmetic mean for the estimation of local mean values, which are optimal only in the mono-edge case, whereas the ratio of exponentially weighted averages (ROEWA) operator is optimal under a stochastic multi-edge model and more appropriate for SAR images. Recently, several researchers [*Chesnaud et al.* 1998, 1999; *Germain and Rfregier* 2001; *Martin et al.* 2004] have developed several active contour methods for edge detection or segmentation of SAR imagery. Their results are promising, but the active contour model they used is parametric. As shown above, it is sensitive to the initial condition and cannot naturally handle changes in the topology of the evolving contour.

In this paper, we propose a novel GAC model based on the ROEWA operator [*Fjortoft et al.*1998] under the criterion of energy minimization. The idea is that the original edge indicator function based on gradients is replaced by a new edge indicator function based on the ROEWA operator. Thus, the capability of detecting edges and the accuracy of locating edges are greatly improved, which makes the model more appropriate for SAR image segmentation. In addition, a “balloon force” term is added to the energy functional of the original model in order to boost the strength for the contour’s evolution.

As a result, the contour's evolution takes less time and the sensitivity to the initial contour is reduced. In the numerical implementation of the model, an unconditionally stable additive operator splitting (AOS) scheme [*Weickert et al.* 1998] and a fast algorithm for re-initialization of the level set function [*Felzenszwalb and Huttenlocher* 2004] are adopted, which not only improve the model's stability, but also speed up the model's convergence remarkably.

2. Background

Let x be the abscissa, y be the ordinate, $\Omega \subset R^2$ be the image domain, $u_0(x,y):\Omega \to R^+$ be a given image, C be a planar contour with the length $L(C)$ and $C(s)=\big(x(s),y(s)\big):[0,L(C)]\to R^2$ be its arc-length parameterization, where s denotes an arc-length variable . The classical GAC model associates the contour C with an energy given by [*Caselles et al.* 1997]

$$\int_0^{L(C)} g(\left|\nabla u_0(C(s))\right|)ds \tag{1}$$

where $\nabla u_0(C(s))$ is the image gradient defined on the contour, $\left|\nabla u_0(C(s))\right|$ denotes the magnitude (modulus) of the gradient. The edge indicator function $g(r):[0,\infty)\to R^+$ is a strictly decreasing function, such that $g(0)=1$ and $g(r)\to 0$ as $r\to\infty$, where r denotes an arbitrary variable. According to the calculus of variations and the gradient descent method, we can obtain the evolution equation for the contour C [*Caselles et al.* 1997]

$$\frac{\partial C}{\partial t}=\left[g\kappa-\left\langle\nabla g,\vec{n}\right\rangle\right]\vec{n} \tag{2}$$

where κ is the mean curvature, $\vec{n}$ is the unit inward normal. Eq. (2) is well-defined because an associated unique viscosity solution exists [*Caselles et al.* 1997]. *Osher* and *Sethian* [1998] introduced the level set method to implicitly solve the contour propagation problem and to deal with topological changes. In the level set framework, the evolving contour C is defined implicitly as the zero level set of an embedding scalar function ϕ, such that $C(t)=\left\{(x,y):\phi(x,y,t)=0\right\}$, where t denotes a time variable. By convention, we assign negative values to the interior and positive values to the exterior of the contour. According to the level set method, Eq.(2) can be written in the level set form as follows [*Caselles et al.* 1997]

$$\frac{\partial \phi}{\partial t} = g\kappa|\nabla\phi| + \nabla g \cdot \nabla\phi \tag{3}$$

3. Proposed Model

3.1. ROEWA Operator

The ROEWA operator, proposed by *Fjortoft et al*. [1998], is based on a linear minimum mean square error (MMSE) filter. In the one-dimensional (1D) case, the linear MMSE filter can be expressed as

$$f(x) = C\exp\{-\rho|x|\} \tag{4}$$

where C is the normalizing constant, ρ is the filtering coefficient. In the discrete case, $f(x)$ can be implemented very efficiently by a causal filter $f_1(x)$ and an anticausal filter $f_2(x)$

$$f(x) = \frac{1}{1+b} f_1(x) + \frac{b}{1+b} f_2(x-1), \quad x = 1, 2, \cdots, N \tag{5}$$

where $f_1(x) = a \cdot b^x H(x)$, $f_2(x) = a \cdot b^{-x} H(-x)$, $0 < b = e^{-\alpha} < 1$, $a = 1 - b$, $H(x)$ is the discrete Heaviside function. If $x \geq 0$, it equals to one, otherwise zero.

Based on the linear MMSE filter, the ROEWA operator can be defined as

$$\begin{cases} r_{X\max}(x,y) = \max\left\{\dfrac{\hat{\mu}_{X1}(x-1,y)}{\hat{\mu}_{X2}(x+1,y)}, \dfrac{\mu_{X2}(x+1,y)}{\mu_{X1}(x-1,y)}\right\} \\ r_{Y\max}(x,y) = \max\left\{\dfrac{\hat{\mu}_{Y1}(x,y-1)}{\hat{\mu}_{Y2}(x,y+1)}, \dfrac{\mu_{Y2}(x,y+1)}{\mu_{Y1}(x,y-1)}\right\} \end{cases} \tag{6}$$

where $\hat{\mu}_{X1}$, $\hat{\mu}_{X2}$, $\hat{\mu}_{Y1}$ and $\hat{\mu}_{Y2}$ are the exponentially weighted averages, which can be obtained by

$$\begin{cases} \hat{\mu}_{X1}(x,y) = f_1(x) * (f(y) \bullet u_0(x,y)) \\ \hat{\mu}_{X2}(x,y) = f_2(x) * (f(y) \bullet u_0(x,y)) \\ \hat{\mu}_{Y1}(x,y) = f_1(y) \bullet (f(x) * u_0(x,y)) \\ \hat{\mu}_{Y2}(x,y) = f_2(y) \bullet (f(x) * u_0(x,y)) \end{cases} \tag{7}$$

where $*$ denotes the convolution in the horizontal direction and $\bullet$ denotes the convolution in the vertical direction. With analogy to gradient-based edge detectors, the magnitude of the ROEWA operator can be defined as

$$\left|r_{\max}(x,y)\right| = \sqrt{r_{X\max}^2(x,y) + r_{Y\max}^2(x,y)} \tag{8}$$

3.2 GAC Model Based on the ROEWA Operator

Based on the ROEWA operator, the new energy functional of the GAC model can be defined as

$$\int_0^{L(C)} g\left(\left|r_{\max}\right|\right)ds + \alpha\int_{\omega} g\left(\left|r_{\max}\right|\right)da \tag{9}$$

where g is the edge indicator function based on the magnitude of the ROEWA operator, which stops the contour in the vicinity of edges

$$g\left(\left|r_{\max}\right|\right) = \frac{1}{1+\left|r_{\max}\right|^2/\lambda^2} \tag{10}$$

where λ is a scaling constant. g is bounded to $[0,1]$, and the more it approaches zero, the better it closes to the edge. In the above functional, the second term is a "balloon force" term to enhance the power for the contour's evolution. As a result, the speed of the contour's evolution is increased and the sensitivity to the initial contour is reduced. α is a constant that aims to keep the contour moving in the proper direction, If $\alpha > 0$, the contour deflates; otherwise inflates. da is the area element and ω is the region inside the contour C.

The calculus of variations and the gradient descent method provides the following evolution equation for the contour C

$$\frac{\partial C}{\partial t} = \left[g\kappa + \alpha g - \left\langle \nabla g, \vec{n}\right\rangle\right]\vec{n} \tag{11}$$

According to the level set method, the evolution equation with respect to the level set function ϕ is

$$\frac{\partial \phi}{\partial t} = g(\kappa+\alpha)\left|\nabla\phi\right| + \nabla g\cdot\nabla\phi \tag{12}$$

where $\kappa = div\left(\frac{\nabla\phi}{|\nabla\phi|}\right)$. To facilitate the numerical calculation, we rewrite Eq.(12) as follows in terms of the property of the divergence $div\left(\varphi\vec{A}\right) = \varphi div\left(\vec{A}\right) + \vec{A}\cdot\nabla\varphi$

$$\frac{\partial \phi}{\partial t} = \left[div\left(g\frac{\nabla\phi}{|\nabla\phi|}\right) + \alpha g\right]\left|\nabla\phi\right| \tag{13}$$

4. Implementation

It is very difficult to directly solve Eq.(13). A numerical scheme is usually adopted to obtain an approximated solution. The first term $div\left(g\nabla\phi/|\nabla\phi|\right)|\nabla\phi|$ in Eq.(13) is a parabolic term. Although this regularizing term is indispensable for the correct evolution, it makes the resulting partial differential equation particularly stiff, numerically. If we use a simple explicit method for numerically evolving the contour, then instability incurs unless very small time steps are applied ($\tau < h^2/4$, where τ is the time step, h is the space step). To overcome this shortcoming, we could use an implicit scheme, which is unconditionally stable and thereby free of the time step limitation. However, a system of equations needs to be solved at each time step, which is complex and time-consuming. On the other hand, the AOS scheme is not only stable but also easy to implement. Therefore, we use this scheme to solve the evolution equation numerically.

4.1 Numerical Scheme

The AOS scheme was introduced by *Weickert et al.* [1998] as an unconditionally stable numerical scheme for the nonlinear diffusion equation in the form of $\partial u_0/\partial t = div(g(|\nabla u_0|)\nabla u_0)$. Comparing it with Eq.(13), we find that there are differences between these two equations and thus their results cannot be directly compared. In fact, if we define the level set function ϕ as a signed distance function (using the Euclidean distance)

$$\phi(x,y)=\begin{cases}-\sqrt{(x-x_0)^2+(y-y_0)^2}, & \text{if } (x,y) \textbf{ is inside } C\\ 0, & \text{if } (x,y) \textbf{ is on } C\\ \sqrt{(x-x_0)^2+(y-y_0)^2} & \textbf{if } (x,y) \textbf{ is outside } C\end{cases} \tag{14}$$

where (x_0,y_0) is the point on the contour C (embedded in the zero level set of ϕ) with the minimum distance from the point (x,y), we obtain $|\nabla\phi|=1$. Consequently, Eq.(13) becomes

$$\frac{\partial\phi}{\partial t}=div\left(g\nabla\phi\right)+\alpha g \tag{15}$$

Eq.(15) can be solved numerically by the AOS scheme in *Weickert et al.*[1998].

By defining two matrix operators: $A_1 = \frac{\partial}{\partial x}\left(g\frac{\partial}{\partial x}\right)$, $A_2 = \frac{\partial}{\partial y}\left(g\frac{\partial}{\partial y}\right)$, we can rewrite Eq.(15) as

$$\frac{\partial \phi}{\partial t} = (A_1 + A_2)\phi + \alpha g \tag{16}$$

Because the edge indicator function g is defined on the magnitude of the ROEWA operator and thereby it is independent of the level set function, the operators A_1 and A_2 keep fixed during the whole evolution process. It is favorable for the numerical calculation of the GAC model.

Let τ be the time step, h be the space step, and $(x_i, y_j) = (ih, jh)$ be the grid points, for $1 \le i \le N_x$, $1 \le j \le N_y$ (N_x and N_y are the pixel numbers in the horizontal and vertical direction, respectively). Furthermore, let $\phi_{i,j}^n = \phi(n\tau, x_i, y_j)$ be an approximation of $\phi(t, x, y)$. The level set function ϕ at the time $n\tau$ is discretized as a matrix $\left[\phi_{ij}^n\right]_{N_x \times N_y}$. On the other hand, variables in the AOS scheme are represented in the form of column vectors. Hence, the matrix $\left[\phi_{ij}^n\right]_{N_x \times N_y}$ should be converted to a column vector. If we scan the pixels lexicographically in a row-major order and concatenate the results in each row, we obtain a column vector ϕ^n with the size $N = N_x \times N_y$. The edge indicator function g can be also changed to the corresponding vector. Based on the above results, the AOS scheme for Eq.(16) is achieved [*Weickert et al.* 1998; *Goldenberg et al.*2001]

$$\phi^{n+1} = \frac{1}{2}\sum_{l=1}^{2}\left[I - 2\tau A_l\right]^{-1}\left(\phi^n + \tau\alpha g\right) \tag{17}$$

The discrete expression of the matrix operators A_l ($l = 1, 2$) should be provided in order to fulfill the calculation of Eq.(17). Assume that $A_l = \left[a_{l,ij}\right]_{N \times N}$, then each element of this matrix is assigned by:

$$a_{l,ij} = \begin{cases} \dfrac{g_i + g_j}{2h^2}, & j \in N(i) \\ -\displaystyle\sum_{k \in N(i)} \dfrac{g_i + g_k}{2h^2}, & j = i \\ 0, & else \end{cases} \tag{18}$$

where $N(i)$ is the set of two neighbors of the pixel i (boundary pixels have only one neighbor) in the

horizontal or vertical direction. Although the expression forms of $a_{1,ij}$ and $a_{2,ij}$ are identical, the actual values are totally different. In fact, $N(i)$ refers to two horizontal neighboring pixels for $a_{1,ij}$, i.e., $i-1$ and $i+1$; whereas for $a_{2,ij}$, $N(i)$ is two vertical neighboring pixels, i.e., $i-N_x$ and $i+N_x$. According to the formulation of A_l ($l=1,2$), one can see that the matrix $I-2\tau A_l$ is tridiagonal and diagonally dominant and therefore can be efficiently solved by the so-called *Thomas algorithm* [*Weickert et al.* 1998].

4.2 Re-initialization of the Level Set Function

As mentioned above, it is necessary to keep the level set function ϕ as a signed distance function such that $|\nabla\phi|=1$ before applying the AOS scheme. However, the level set function will deviate from the signed distance function during the evolution. To avoid this problem, ϕ should be re-initialized to a signed distance function before each iteration. There are several distance transform algorithms for the level set re-initialization. One of the most common approaches is the fast marching (FM) algorithm proposed by *Sethian* [1996]. The FM algorithm utilizes an efficient insert-sort procedure based on heaps and has the complexity of $O(N\log N)$, where N is the pixel number. Recently, a new distance transform algorithm was proposed by *Felzenszwalb and Huttenlocher* [2004] and used by *Papandreou and Maragos* [2007]. It can rapidly re-initialize ϕ to a distance function with the complexity of $O(N)$. Furthermore, their algorithm is very easy to implement. Hence, we use it as the re-initialization tool. The basic idea of this algorithm is as follows.

Let $\Omega=\{1,\cdots,N_x\}$ be a 1D grid, and $f:\Omega\to R$ an arbitrary function on the grid. The squared Euclidean 1D distance transform of f is given by $D_f(x)=\min_{x'\in\Omega}\{(x-x')^2+f(x')\}$. Note that for each point $x'\in\Omega$, there is a constraint that the distance transform of f is bounded by a parabola rooted at $(x',f(x'))$. In fact, the distance transform is defined by the lower envelope of these parabolas and the value of the distance transform at x is simply the height of the lower envelope at that point. For the two-dimensional (2D) grid $\Omega=\{1,\cdots,N_x\}\times\{1,\cdots,N_y\}$, the 2D distance transform of f under

the squared Euclidean distance is given by: $D_f(x,y) = \min_{x',y' \in \Omega} \left\{ (x-x')^2 + (y-y')^2 + f(x',y') \right\}$. Note that the first term does not depend on y' and the second term does not depend on x', this 2D distance transform can be separated, i.e., $D_f(x,y) = \min_{x' \in \Omega} \left\{ (x-x')^2 + D_{f|x'}(y) \right\}$, where $D_{f|x'}(y) = \min_{y' \in \Omega} \left\{ (y-y')^2 + f(x',y') \right\}$. Thus the 2D transform can be computed by firstly performing 1D transforms along each column of the grid, and then performing 1D transforms along each row of the grid [*Felzenszwalb and Huttenlocher* 2004].

4.3 Segmentation Algorithm

Based on the proposed model, a SAR image segmentation algorithm is proposed. The main steps of the algorithm include (1) initialize ϕ^0 (its zero level set corresponds to the initial contour) and letn=0; (2) compute the edge indicator function g by Eq.(10); (3)solve the evolution equation by Eq.(17) to obtain the updated level set function ϕ^{n+1}; (4)reinitialize the level set function ϕ^{n+1} as a signed distance function; and (5)check whether ϕ^{n+1} is converged or the maximum iteration is achieved. If not, let $n = n+1$, and repeat.

Let the zero level set of $\phi^n = A$ and $\phi^{n+1} = B$, the convergence condition is $H(A,B) \le T$, where T is a threshold, usually $T = h$, and $H(A,B) = \max\left(h(A,B), h(B,A)\right)$ is the Hausdorff distance between A and B. Here, $h(A,B) = \max_{a \in A} \min_{b \in B} \|a-b\|$ is the directed Hausdorff from A to B; and $h(B,A) = \max_{b \in B} \min_{a \in A} \|b-a\|$ is the directed Hausdorff from B to A.

To facilitate the implementation, the parameters involved in the segmentation algorithm are explained as follows. In Eq. (5), a and b are two parameters of the ROEWA filter , which are used to control the edge details extracted from SAR images. According to results presented in *Fjortoft et al.* [1998], $a = 0.3$, $b = 0.7$ are good enough for most SAR images. In Eq. (10), λ is a scaling constant for the function g, which is used to adjust the value of g. If $|\mathbf{r}_{\max}|$ is smaller, β should be smaller and vice versa. β is set to 0.1 in the general case. In Eq. (9), α is a coefficient that aims to keep the contour moving in the proper direction. If $\alpha > 0$, the contour deflates; otherwise inflates. Theoretically,

α isn't bounded to any values. However, we often bound it to [-1, 1] from the engineering point of view. If a larger value is assigned to it, the contour's evolving power is bigger and the speed is faster, which often make the contour surpass actual edges. On the contrary, if a smaller value is set, the contour's evolving power is insufficient to make the contour reach actual edges. As a result, α should be carefully adjusted for different images. In Eq. (18), h is the space step for the difference equation. Usually, $h = 1$. In Eq. (17), τ is the time step for the difference equation. We mention that the choice of the time step is a compromise between the accuracy and the efficiency. Choosing larger step can speed up the evolution, but may also cause errors in the edge location. Usually, the time step τ should be less than 10.0.

5. Results and Discussion

Five RADARSAT-2 images with dimensions of 435×342 pixels were used in this study. The experiments were carried out with MATLAB V7.4 on a PC with a Pentium IV 1.8 GHz CPU and 1 GB RAM. The kernel code for the AOS scheme was implemented in C++. The parameters used in the experiments are as follows: $b = 0.7$, $a = 1 - b = 0.3$, $\lambda = 0.1$, $h = 1$, $\tau = 5$ and the "balloon force" parameter α is adjusted according to the specific image. The ENIL of these images is 1. The equivalent look number of all the image extracts is 1. The reflectivity contrast of these images are 19.8717, 23.3076, 14.4959, 21.5752 and 16.346, respectively. The initial contour was set to a rectangle very close to the image boundary. The parameter α was set to 0.85, 0.80, 0.83, 0.90 and 0.90, respectively. The execution time for image processing was about 12 seconds. Fig. 1 shows the segmentation results, which demonstrate that the algorithm performs well and fast. The settings for the initial contour are almost identical for all images, which indicate that the algorithm is not sensitive to the initial conditions as is the classical Snakes algorithm.

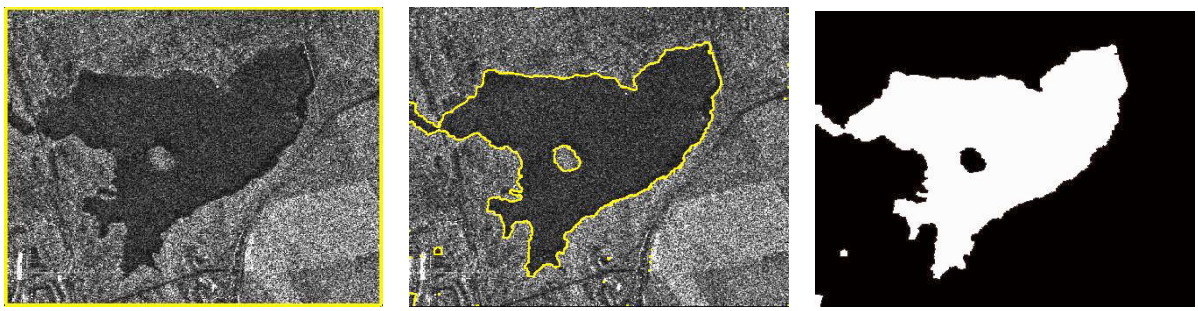

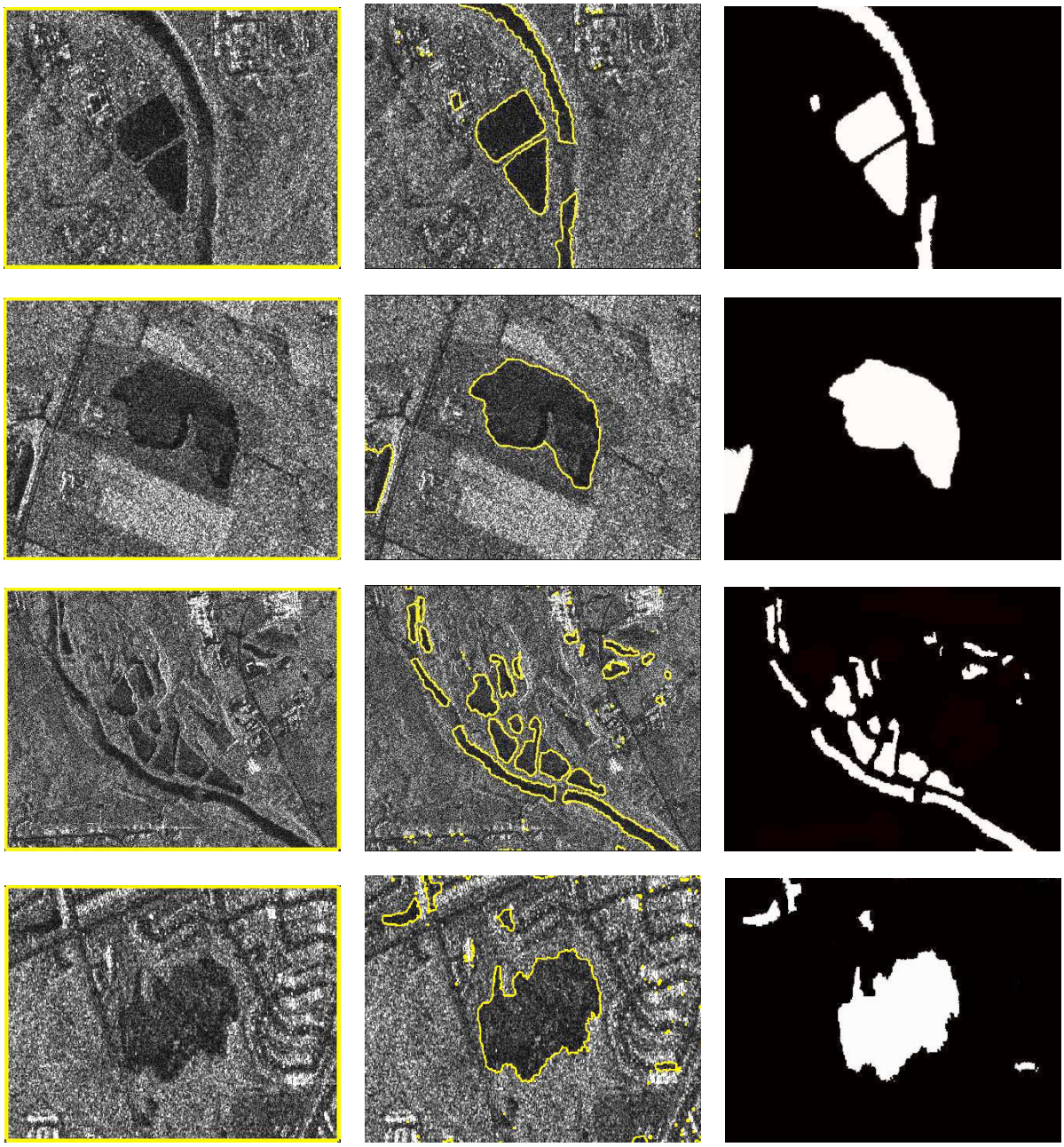

(a) (b) (c)

Fig. 1 Segmentation results of RADARSAT-2 images using our method. (a) Original image with initial contours; (b) Detected contours; (c) Segmentation results.

6. Performance Evaluation

6.1 Quality Evaluation

Objective assessment of an algorithm's performance requires testing the consistency between the segmentations it produces and the cartoon model upon which it is based. The cartoon model is an

image model where a real image with detailed contents is represented by a large scale piecewise smooth image with several gray levels. This means that segments must be homogeneous and statistically distinct from their neighbors. The latter condition can be forced by segment merging, so that segments need only be tested for homogeneity. Here we adopt two methods from *Caves et al.* [1998] to carry out such tests for an arbitrary segmentation.

Caves et al. [1998] defined two quality criteria for real images: intensity variance of the ratio image σ_{RI}^2 and normalized likelihood ratio of log intensity ratio image D. Suppose the original image u_0, the segmented image u_{seg}, and the size of image is $m \times n$, then the ratio image RI is defined:

$$RI = u_{seg} / u_0 \tag{19}$$

The ratio image shows the residual structure of the original image after the region segmentation, which can be used to measure the performance of segmentation. Based on the ratio image, two quality criteria can be defined as follows:

$$\sigma_{RI}^2 = \sum_{k=1}^{L} \frac{n_k}{mn-1} \left(\overline{RI_k^2} - \overline{RI_k}^2 \right) \tag{20}$$

$$D = \sum_{k=1}^{L} \frac{n_k}{mn} \overline{\ln RI_k} \tag{21}$$

where L is the sub-region numbers of the ratio image, RI_k is the k-th sub-region of the ratio image, n_k is the pixel numbers of RI_k, $\overline{RI_k^2}$ and $\overline{RI_k}^2$ are the mean of square and square of mean of RI_k separately. The two parameters are zero only when all pixels have the same intensity. Therefore the segmented region is homogeneous when these two parameters approach zero. The evaluation results of segmentation quality for the five images demonstrated the values of σ_{RI}^2 and D with (0.14 and 0.23) for image 1, (0.15 and 0.25) for image 2, (0.12, 0.22) for image 3, (0.17, 0.24) for image 4, and (0.16, 0.25) for image 5.

A series of different size test images from a single scene were produced by pixel replication to evaluate computing performance. The time taken by the algorithm to process these images is 1.7 sec. (64×64 pixels), 6.1 sec. (128×128 pixels), 26.5 sec. (256×256 pixels), 143.6 sec. (512×512 pixels) and 864.8 sec. (1024×1024 pixels), respectively.

6.2 Comparison

In order to demonstrate the effectiveness of the proposed segmentation algorithm, we compared it with a traditional edge-based algorithm on the basis of watershed segmentation algorithm (see [*Fjortoft et al.* 1998] for detailed implementation), which is similar to our GAC model based on ROEWA (MGAC) procedure. Quantitative comparison of the two segmentation algorithms indicates that the values of σ_{RI}^2 and D in our method (0.11 and 0.21) are smaller than those in the watershed algorithm (0.24 and 0.35), which verifies the superior segmentation quality of our approach. Also our method is easier to use than the watershed method. In particular, the watershed technique usually needs thresholding to eliminate false edges before the watershed segmentation and needs regions merging to acquire reasonable segmentation results after the watershed transformation. In contrast, our method can get final segmentation results directly and needs no pre- and post-processing.

7. Concluding Remarks

In this paper, we have presented a novel geodesic active contour model based on SAR image edge detectors under the criterion of energy minimization. The experimental results obtained by using real RADARSAT-2 images show that our segmentation algorithm has several advantages over traditional approaches. Firstly, it can locate the object edges accurately and produce homogeneous segmentation regions. Secondly, it takes less computational time. Finally, it is more robust to initial conditions than the classical Snakes algorithm. The proposed method is limited, however, to handle less than two classes, etc. Designing a more efficient algorithm based on the multigrid method [*Papandreou and Maragos* 2007] to speed up the convergence would be an interesting avenue for further research. In addition, using the statistical properties of SAR images more explicitly should produce more accurate segmentation.

References

Bovik A. C., 1988. On detecting edges in speckle imagery, *IEEE Trans. Acoust., Speech, Signal Processing*, vol. 36, no. 10, pp. 1618–1627.

Caselles V., R. Kimmel, and G. Sapiro, 1997. Geodesic active contours, *Int. J. Computer Vision,* vol. 22, no. 1, pp. 61-79.

Caves R., S. Quegan, and R. White, 1998. Quantitative comparison of the performance of SAR segmentation algorithms, *IEEE Trans. Image Process.*. vol. 7, no. 11, pp. 1534-1546.

Chesnaud C., V. Page, and P. Refreger, 1998. Robustness improvement of the statistically independent region snake-based segmentation method, *Opt. Lett.*, vol. 23,no. 7, pp. 488–490.

Chesnaud C., P. Refregier, and V. Boule, 1999. Statistical region snake-based segmentation adapted to different physical noise models, *IEEE Trans. Pattern Anal. Machine Intell.,* vol. 21, no.11, pp. 1145-1157.

Cohen L. D., 1991. On active contour models and balloons, *CVGIP: Image Understanding*, vol. 53, no. 2, pp. 211-218.

Collins M. J. and E. B. Kopp, 2008. On the design and evaluation of multiobjective single-channel SAR image segmentation algorithms, IEEE Trans. on Geosc. and Remote Sensing, vol.46, no. 6, pp.1836-1846.

Cook R., I. McConnell, C. Oliver and E. Welbourne, 1994. MUM (Merge using moments) segmentation for SAR images, *SPIE: SAR Data Processing for Remote Sensing*, vol. 2316, pp.92-103.

Felzenszwalb P. and D. Huttenlocher, 2004. *Distance Transforms of Sampled Functions*, Technical Report TR2004-1963, Cornell Comput. Inf. Sci., Cornell Univ., Ithaca, NY.

Fjortoft R., A. Lopes, P. Marthon, and E. C. Castan, 1998. An optimal multiedge detector for SAR image segmentation, *IEEE Trans. Geosci. Remote Sensing*, vol. 36, no. 3, pp. 793-802.

Fjortoft R., Y. Delignon, W. Pieczynski, and F. Tupin, 2003. Unsupervised classification of radar images using hidden Markov chains and hidden Markov random fields, *IEEE Trans. Geosci. Remote Sensing*, vol. 41, no. 3, pp. 675-686.

Germain O. and P. Refregier, 2001. Edge location in SAR images: performance of the likelihood ratio filter and accuracy improvement with an active contour approach, IEEE *Trans. Image Process.*, vol. 10, no. 1, pp. 72-78.

Goldenberg R., R. Kimmel, E. Rivlin, and M. Rudzsky, 2001. Fast geodesic active contours, *IEEE Trans. Image Process.*, vol. 10, no. 10, pp. 1467-1475.

He Z, Lu J, and Kuang G, 2009. SAR image segmentation based on the global active contour model, *Progress in Nature Science*, Vol.10, no.3, pp. 344-360.

Kass M., A. Withkin, and D. Terzopoulos, 1988. Snakes: active contour models, *Int. J. Computer Vision,* vol. 1, no. 4, pp. 321-331.

Martin P., P. Refregier, and F. Goudail, et al, 2004. Influence of the noise model on level set active contour segmentation, *IEEE Trans. Pattern Anal. Machine Intell.,* vol. 26, no.6, pp. 799-803.

Oliver C. J., D. Blacknell and R. G. White, 1996. Optimal edge detection in SAR, *IEE Proc. Radar, Sonar Naving*. vol. 143, no. 1, pp. 31-40.

Osher S., and J. A. Sethian, 1998. Fronts propagating with curvature-dependent speed: algorithms based on Hamilton-Jacobi formulation, *J. Computational Physics*. vol. 79, no. 1, pp. 12-49.

Papandreou G. and P. Maragos, 2007. Multigrid geometric active contour models, *IEEE Trans. Image Process.*, vol. 16, no. 1, pp. 229-240.

Schultz, G. A., and E. T. Engman, 2000. *Remote Sensing in Hydrology and Water Management*, Springer-Verlag, Berlin, Germany.

Sethian J. A., 1996. A fast marching level set method for monotonically advancing fronts, *Proc. National Academic Science*, vol. 93, no. 4, pp. 1591-1595.

Shen J. and S. Castan, 1992. An optimal linear operator for step edge detection, *CVGIP: Graph., Models, Image Process.*, vol. 54, no. 2, pp. 112–133.

Shu, Y. M., J. Li, and G. Gomes, 2010. Shoreline extraction from RADARSAT-2 intensity imagery using a narrow band level set segmentation approach, *Marine Geodesy,* vol. 33, no. 2&3, pp. 187-203.

Touzi R., A. Lopes, and P. Bousquet, 1988. A statistical and geometrical edge detector for SAR images, *IEEE Trans.Geosci. Remote Sensing*, vol. 26, no. 6, pp. 764-773.

Weickert J., B. Romeny, and M. Viergever, 1998. Efficient and reliable schemes for nonlinear diffusion filtering, *IEEE Trans. Image Process.*, vol. 7, no. 3, pp. 398-410.

Zhu S. C.and A. Yuille, 1996. Region competition: unifying snakes, region growing, and Bayes/MDL for multiband image segmentation, *IEEE Trans. Pattern Anal. Machine Intell*. vol. 18, no. 9, pp. 884-900.